

MÉTODOS NUMÉRICOS EN INGENIERÍA
R. Abascal, J. Domínguez y G. Bugeda (Eds.)
© SEMNI, España 1999

ANALYSIS OF CONCRETE SLABS SUPPORTED ON SOIL

Joaquim Barros

- Departamento de Engenharia Civil
 - Escola de Engenharia da Universidade do Minho
 - Azurém, 4800 Guimarães, Portugal
- e-mail: barros@eng.uminho.pt

Palabras clave: Material non-linear analysis, steel fibre reinforced concrete, fracture energy, strain softening, strain stiffening, soil load bearing capacity

Resumen: *A numerical model for material non-linear analysis of concrete slabs supported on soil is described in this work. In this model, the cracked concrete is regarded as cracks with concrete between cracks. The behaviour of the concrete between cracks is simulated by the conventional theory of plasticity. The behaviour of the cracks is defined by their constitutive laws using the concrete fracture properties. Smeared multifixed and rotating crack models are available in the model.*

Concrete can be reinforced with sets of smeared bars of different materials and geometric properties, as well as with discrete steel fibres. A tension-stiffening model that takes into account the concrete fracture properties and the reinforcement characteristics is used for the reinforced cracked concrete.

Main effects of the fibre reinforcement are reproduced in the model, introducing the material fracture energy and a convenient softening law in the crack constitutive law, and using a new stress-strain relationship for the behaviour in compression.

Soil supporting the concrete slab is simulated with springs perpendicular to the slab middle surface. The soil non-linear behaviour and the loss of contact between slab and soil are accounted for.

Concrete slabs supported on soil are analysed with the model proposed. Safety of wire mesh reinforced concrete slabs and steel fibre reinforced concrete slabs is discussed. A comparison with conventional design methods is performed. The influences of the soil load bearing capacity, as well as the loss contact between soil and slab on the behaviour of slab-soil system are analysed.

1. INTRODUCTION

In the last two decades the increase on computer power and software facilities, as well as a significant effort on the experimental research about material constitutive laws, contributed to the development of several computer programs for numerical simulation of concrete structures. However, numerical simulation of a slab supported on soil remains a difficult task. Accurate simulation of the behaviour of this kind of structures is only feasible if the numerical model takes into account the non-linear behaviour of the concrete, soil and reinforcement, as well as the soil-slab interaction.

In recent years, steel fibre reinforced concrete (*SFRC*) has been extensively applied in industrial floors with recognised economical and technical benefits^{1,2,3}. Some experimental research with concrete slabs on soil (or other similar support like rubber or cork layers⁴) has been performed in order to evaluate the enhance in the load carrying capacity and concrete cracking behaviour due to fibre reinforcement⁵. These tests revealed that steel fibres can replace the conventional reinforcement in industrial floors.

The first approach to design slabs on soil was proposed by Westergaard⁶, using the elasticity theory. Since materials are assumed linear elastic and the design condition is based on concrete tensile strength, very thick plain concrete slabs are obtained with this approach. In the beginning of sixties Losberg⁷ and Meyerhof⁸ developed similar theories based on the yield line theory for reinforced concrete laminar structures. However, these theories are not able to reproduce the deformational behaviour of a slab-soil system until collapse load. Nowadays, design of *SFRC* slabs is usually performed with models devised for structures of conventional concrete, wherefore fibre-reinforcing effects are not simulated appropriately. Therefore, the numerical simulation of the behaviour of *SFRC* slabs supported on soil is an actual challenge for the computational mechanics community.

The present work aims to contribute to the on going research effort on the numerical simulation of concrete slabs supported on soil. Concrete slabs can be reinforced with smeared steel roads and/or steel fibres. Main changes on concrete behaviour due to fibre reinforcement were evaluated from experimental research and introduced in the material constitutive laws⁹. A design of a concrete slab on soil using a linear elastic finite element computer code is compared with an analysis using the numerical model described in this work. The influence of simulating the loss of contact between the slab and the soil and the influence of the soil constitutive law in a material non-linear analysis of a slab supported on soil are discussed.

2. NUMERICAL MODEL

2.1 Introduction

In the present work concrete cracking is simulated under the framework of smeared crack concepts. Smeared crack concepts can be categorised into fixed, multifixed and rotating crack models^{9,10,11}. These crack models are available in the computational code developed.

According to the present model the total strain increment of cracked concrete, $\Delta \underline{\underline{\varepsilon}}$, is due to the strain increment in the fracture zone, $\Delta \underline{\underline{\varepsilon}}^{cr}$ (the width of the finite element over which the micro-cracks are smeared out) and to the strain increment in concrete between cracks, $\Delta \underline{\underline{\varepsilon}}^{co}$,

$$\Delta \underline{\underline{\varepsilon}} = \Delta \underline{\underline{\varepsilon}}^{co} + \Delta \underline{\underline{\varepsilon}}^{cr}. \quad (1)$$

In order to simulate the progressive damage induced by plasticity and cracking, a plane shell element is discretized in layers throughout element thickness. Each layer is considered in plane stress state. The concrete shell can be reinforced with conventional smeared steel bars or/and steel fibres. The plane shell was formulated under the well-known Reissner-Mindlin theory¹².

2.1 Concrete constitutive laws

For the concrete between cracks, stress and strain increment vectors are related by the constitutive law

$$\Delta \underline{\underline{\sigma}} = \underline{\underline{D}}^{co} \Delta \underline{\underline{\varepsilon}}^{co} \quad (2)$$

where $\underline{\underline{D}}^{co}$ is the concrete tangent constitutive matrix,

$$\underline{\underline{D}}^{co} = \begin{bmatrix} \underline{\underline{D}}_{mb}^{co} & \underline{\underline{\phi}} \\ \underline{\underline{\phi}} & \underline{\underline{D}}_s^{co} \end{bmatrix}, \quad (3)$$

$\underline{\underline{D}}_{mb}^{co}$ is the in-plane material stiffness matrix and $\underline{\underline{D}}_s^{co}$ is the out-plane shear stiffness matrix.

2.2.1 - Linear elastic uncracked concrete

For homogeneous, isotropic and linear elastic materials, the submatrix \underline{D}_{mb}^{co} in (3) is the elastic in-plane material stiffness matrix, $\underline{D}_{mb,e}^{co}$,

$$\underline{D}_{mb,e}^{co} = \frac{E_c}{1-\nu_c^2} \begin{bmatrix} 1 & \nu_c & 0 \\ \nu_c & 1 & 0 \\ 0 & 0 & \frac{1-\nu_c}{2} \end{bmatrix} \quad (4)$$

where E_c is the instantaneous modulus of elasticity and ν_c is Poisson's coefficient. In this work, the material behaviour on transverse shear deformation is considered on linear elastic state. Therefore, the material stiffness matrix in shear has the form

$$\underline{D}_s^{co} = \underline{D}_{s,e}^{co} = F G_c \begin{bmatrix} 1 & 0 \\ 0 & 1 \end{bmatrix} \quad (5)$$

where G_c is the concrete transversal modulus of elasticity and F is a correction shear factor¹³.

2.2.2 - Linear elastic cracked concrete

For linear elastic cracked concrete (*ecr*), the submatrix \underline{D}_{mb}^{co} in (3) is designated by $\underline{D}_{mb,ecr}^{co}$, defined by the following expression¹⁰

$$\underline{D}_{mb}^{co} = \underline{D}_{mb,ecr}^{co} = \left\{ \underline{D}_{mb,e}^{co} - \underline{D}_{mb,e}^{co} \hat{N} \left[\hat{D}^{cr} + \hat{N}^T \underline{D}_{mb,e}^{co} \hat{N} \right]^{-1} \hat{N}^T \underline{D}_{mb,e}^{co} \right\} \quad (6)$$

where \hat{N} is the matrix that defines the direction of the cracks developed in a sampling point (see Figure 1), and \hat{D}^{cr} is the matrix which accounts for the constitutive law of the cracks. Each crack is governed by the following constitutive relationship

$$\Delta \underline{s}^{cr} = \underline{D}^{cr} \Delta \underline{e}^{cr} \quad (7)$$

where $\Delta \underline{s}^{cr}$ is the crack stress vector (see Figure 1)

$$\Delta \underline{s}^{cr} = \begin{bmatrix} \Delta s_{nn}^{cr} & \Delta s_{nt}^{cr} \end{bmatrix}^T \quad (8)$$

$\Delta \underline{e}^{cr}$ is the crack strain vector

$$\Delta \underline{e}^{cr} = \begin{bmatrix} \Delta e_{nn}^{cr} & \Delta \gamma_{nt}^{cr} \end{bmatrix}^T \quad (9)$$

and

$$\underline{D}^{cr} = \begin{bmatrix} D_I^{cr} & 0 \\ 0 & D_{II}^{cr} \end{bmatrix} \quad (10)$$

is the crack material stiffness matrix, where D_I^{cr} and D_{II}^{cr} are the mode I and mode II stiffness modulus of a smeared single crack, respectively.

D_I^{cr} is characterised by the fracture parameters, namely, the tensile strength, f_{ct} , the fracture energy, G_f , the shape of the softening law and the crack band width¹⁰, l_b . Considerable experimental and numerical work has been done to characterise the fracture parameters of plain concrete. However, for *SFRC* the research on its post-cracking behaviour is still scarce. Fibre reinforcement mechanisms are reflected, mainly, on the fracture energy and on the shape of the softening branch. The remainder fracture parameters are only marginally affected by fibre addition into concrete.

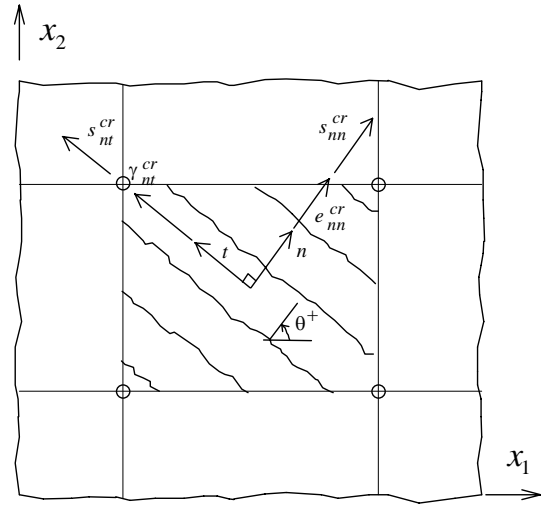


Figure 1 : Crack stress and crack strain components.

In order to evaluate the fracture energy and the shape of the softening diagram for *SFRC*, sets of four point bending notched beam tests were carried out under displacement control¹⁴. It was tested sets of specimens reinforced with 0, 30, 45 and 60 Kg/m³ of hooked ends Dramix steel fibres¹⁵. Based on the results obtained, the following expressions were proposed

$$\frac{G_f}{G_{fo}} = 19.953 + 3.213W_f \quad \text{with } 1.25 \leq W_f \leq 2.5 \quad (11)$$

for concrete reinforced with *ZP30/.50* fibres (30 mm of length and 0.5 mm of diameter) and

$$\frac{G_f}{G_{fo}} = 1.0 + 13.159W_f^{1.827}, \quad (12)$$

for concrete reinforced with *ZX60/.80* fibres (60 mm of length and 0.8 mm of diameter),

where G_{fo} is the fracture energy of the corresponding plain concrete, which can be evaluated from RILEM recommendations¹⁶ and W_f is the fibre weight percentage in the mixture.

The shape of the softening diagram of *SFRC* was adjusted by performing numerical simulations of the four point bending notched beam tests. This numerical simulation revealed⁹ that a trilinear diagram (see Figure 2a) is appropriate to reproduce the post-peak tensile behaviour of *SFRC*, but the simplified bilinear diagram shown in Figure 2b is also adequate.

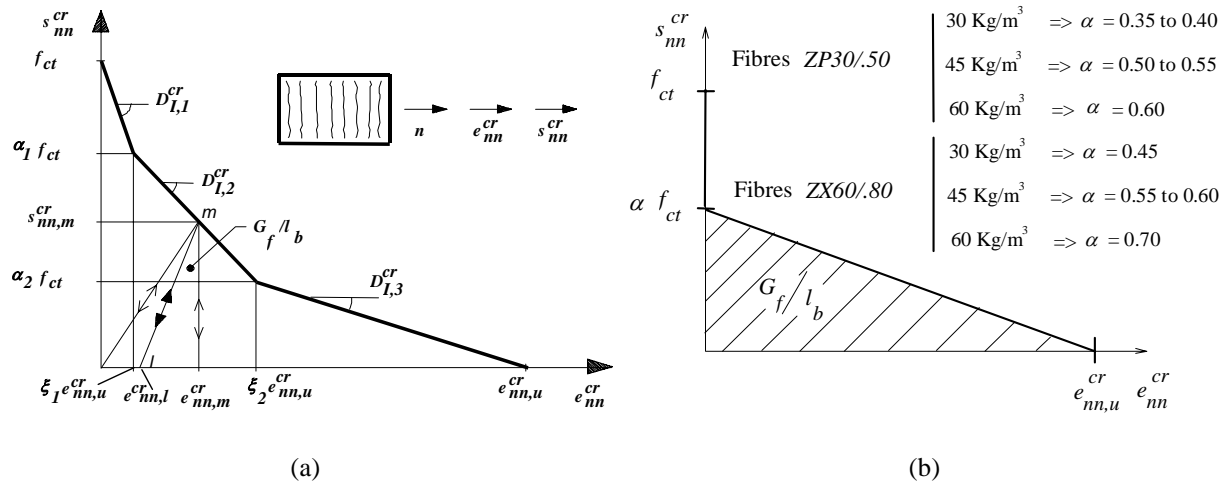


Figure 2 : Trilinear (a) and bilinear (b) softening diagram for hooked-ends steel fibre reinforced concrete.

Ranges of values for defining the characteristic points of the trilinear softening diagram are included in Table 1. More experimental and numerical work should be done to calibrate these ranges of values.

Parameters	Fibre type					
	ZP30/.50			ZX60/.80		
	Fibre content (Kg/m ³)			Fibre content (Kg/m ³)		
	30	45	60	30	45	60
$\xi_1 (\times 10^{-3})$	7 - 9	4 - 6	3 - 5	3 - 5	3 - 5	10 - 100
α_1	0.35 - 0.45	0.55 - 0.65	0.6 - 0.65	0.4 - 0.5	0.6 - 0.7	0.65 - 0.75
ξ_2	0.2 - 0.3	0.25 - 0.35	0.3 - 0.4	0.15 - 0.25	0.15 - 0.25	0.3 - 0.5
α_2	0.1 - 0.2	0.15 - 0.25	0.15 - 0.25	0.2 - 0.3	0.25 - 0.35	0.25 - 0.35

Table 1: Ranges of values for defining the characteristic points of the trilinear softening law of *SFRC*. Residual strain at crack closing is higher in fibrous concrete than in plain concrete¹⁷. To model this behaviour it is proposed the law (see Figure 2a)

$$e_{nn,l}^{cr} = \eta e_{nn,m}^{cr} \quad (13)$$

where $e_{nn,m}^{cr}$ is the maximum attained crack strain normal to the crack, and

$$\eta = \left[1 - \exp(-1000 e_{nn,m}^{cr}) \right] \left[1 - \exp\left(-\frac{W_f}{C} \frac{l_f}{d_f}\right) \right] \quad (14)$$

with l_f and d_f being the fibre length and fibre diameter. For C parameter it is advanced a value of 165, but more experimental research is needed to calibrate this parameter.

The fracture mode II modulus, D_{II}^{cr} , is obtained from the expression¹⁰

$$D_{II}^{cr} = \frac{\beta}{1 - \beta} G_c \quad (15)$$

where β is the shear retention factor determined from

$$\beta = \left[1 - \frac{e_{nn}^{cr}}{e_{nn,u}^{cr}} \right]^p \quad (p=1, 2 \text{ or } 3) \quad (16)$$

for plain concrete, with $e_{nn,u}^{cr}$ being the ultimate normal crack strain (see Figure 2), and

$$\beta = \exp\left(-\frac{M}{W_f} \frac{d_f}{l_f} \frac{e_{nn}^{cr}}{e_{nn,u}^{cr}}\right) \quad (17)$$

for *SFRC*. M parameter must be evaluated from experimental research. Based on the reduced data available, a value of 980 is proposed for M .

The shear retention factor for conventionally reinforced concrete is evaluated from an expression proposed by Cervenka¹⁸

$$\beta = -\frac{\ln\left(\frac{e_{nn}^{cr}}{C_1}\right)}{C_2} \quad (18)$$

with

$$C_1 = 7 + 5 \frac{\rho_{eq,ef}^e - 0.005}{0.015}, \quad C_2 = 10 - 2.5 \frac{\rho_{eq,ef}^e - 0.005}{0.015} \quad (19)$$

where $\rho_{eq,ef}$ is the equivalent effective reinforcement⁹

$$\rho_{eq,ef} = \sum_{i=1}^{nr} \rho_{i,ef} \cos^4 \theta_i \quad (20)$$

nr is the number of sets of reinforcing layers crossing the crack, $\rho_{i,ef}$ is the effective reinforcing ratio¹⁹ of layer i and θ_i is the angle between the reinforcing layer i and the crack direction.

2.2.3 - Elasto-plastic uncracked concrete

For elasto-plastic (ep) uncracked concrete, the in-plane material stiffness matrix \underline{D}_{mb}^{co} in (3) is defined by

$$\underline{D}_{mb}^{co} = \underline{D}_{mb,ep}^{co} = \underline{D}_{mb,e}^{co} - \frac{\underline{D}_{mb,e}^{co} \underline{a} \underline{a}^T \underline{D}_{mb,e}^{co}}{h + \underline{a}^T \underline{D}_{mb,e}^{co} \underline{a}} \quad (21)$$

where \underline{a} is the flow vector and h is the hardening modulus²⁰. The hardening modulus depends on the equivalent stress-plastic strain relationship used for concrete in compression. For plain concrete this relationship is based on the stress-strain relationship proposed by CEB-FIP Model Code 1990¹⁹. However, the uniaxial compression tests under displacement control have shown that this expression is not appropriate to simulate the post-peak behaviour of $SFRC$ ⁹. Based on the results obtained with uniaxial compression tests a new expression was proposed for $SFRC$ ¹⁴. In the plasticity approach concrete strain, ε^{co} , is decomposed into an elastic, ε_e^{co} , and a plastic, ε_p^{co} , contributions. Inserting this decomposition into the expression proposed for $SFRC$ ¹⁴ holds

$$\sigma_c \left(\frac{q}{\varepsilon_{cl}^{co}} \varepsilon_p^{co} + A - \frac{f_c}{B} \right) + \sigma_c^2 \frac{q}{B} + \sigma_c p \left(\frac{\sigma_c}{B} + \frac{\varepsilon_p^{co}}{\varepsilon_{cl}^{co}} \right)^{\left(1 + \frac{A}{p}\right)} - f_c \frac{\varepsilon_p^{co}}{\varepsilon_{cl}^{co}} = 0 \quad (22)$$

with

$$A = \frac{E_{c1}}{E_c}, \quad q = 1 - p - A, \quad B = E_c \varepsilon_{c1}^{co} \quad (23)$$

where

$$\varepsilon_{c1}^{co} = \varepsilon_{c10}^{co} + 0.0002W_f, \quad (24)$$

$$p = 1.0 - 0.919 \exp(-0.394W_f) \quad (25)$$

for *ZP30/.50* fibres and

$$\varepsilon_{c1}^{co} = \varepsilon_{c10}^{co} + 0.00026W_f, \quad (26)$$

$$p = 1.0 - 0.722 \exp(-0.144W_f) \quad (27)$$

for *ZX60/.80* fibres. E_{c1} is the secant modulus of elasticity¹⁹ and ε_{c10}^{co} and ε_{c1}^{co} are the strain at peak stress of plain concrete (2.2×10^{-3} according to CEB-FIP Model Code 1990¹⁹) and *SFRC*⁹. For a given concrete plastic strain, the concrete stress is computed from (22) by using the Newton-Raphson method. The concrete hardening modulus is obtained by deriving (22) in order to concrete plastic strain, resulting

$$h = \frac{\frac{f_c}{\varepsilon_{c1}^{co}} - \sigma_c \frac{q}{\varepsilon_{c1}^{co}} - \sigma_c \frac{p}{\varepsilon_{c1}^{co}} \left(1 + \frac{A}{p}\right) \left(\frac{\sigma_c}{B} + \frac{\varepsilon_p^{co}}{\varepsilon_{c1}^{co}}\right)^{\left(\frac{A}{p}\right)}}{\frac{q}{\varepsilon_{c1}^{co}} \varepsilon_p^{co} + A - \frac{f_c}{B} + 2\sigma_c \frac{q}{B} + p \left(\frac{\sigma_c}{B} + \frac{\varepsilon_p^{co}}{\varepsilon_{c1}^{co}}\right)^{\left(1 + \frac{A}{p}\right)} + \sigma_c \frac{p}{B} \left(1 + \frac{A}{p}\right) \left(\frac{\sigma_c}{B} + \frac{\varepsilon_p^{co}}{\varepsilon_{c1}^{co}}\right)^{\left(\frac{A}{p}\right)}}. \quad (28)$$

For fibres contents used in industrial floors, experimental research has shown^{21,22} that the shape of the yield surface of *SFRC* under biaxial stress state is similar to the yield surface of the corresponding plain concrete. The yield surface proposed by Owen and Figueiras²³

$$f_c(\underline{\sigma}_c, k_c) = \left(\underline{\sigma}_c^T \underline{P}_c \underline{\sigma}_c\right)^{1/2} + \underline{p}_c^T \underline{\sigma}_c - \bar{\sigma}_c(k_c) = 0 \quad (29)$$

is used in the present work for plain and fibrous concrete. $\bar{\sigma}_c(k_c)$ is the equivalent compressive stress, with k_c being the hardening parameter, associated to the equivalent plastic strain rate or with the plastic work rate, \underline{P}_c denoting the projection matrix²⁴

$$\underline{P}_c = \begin{bmatrix} a & b & b & 0 \\ b & a & b & 0 \\ b & b & a & 0 \\ 0 & 0 & 0 & c \end{bmatrix} \quad (30)$$

and \underline{p}_c being the projection vector,

$$\begin{aligned} \underline{p}_c &= d \underline{p}_1 \\ &= d [1 \quad 1 \quad 1 \quad 0]^T. \end{aligned} \quad (31)$$

Scalar parameters a , b , c and d are defined as

$$a = \left(\frac{0.355}{2} \right)^2, \quad b = \left(\frac{0.355}{2} \right)^2 - \frac{1.355}{2}, \quad c = 3 \times 1.355, \quad d = \frac{0.355}{2}. \quad (32)$$

2.2.4 - Elasto-plastic cracked concrete

For elasto-plastic cracked concrete (*epcr*), the submatrix \underline{D}_{mb}^{co} of (3) is obtained from the following expression

$$\underline{D}_{mb}^{co} = \underline{D}_{mb,epcr}^{co} = \left\{ \underline{D}_{mb,ep}^{co} - \underline{D}_{mb,ep}^{co} \hat{\underline{N}} \left[\hat{\underline{D}}^{cr} + \hat{\underline{N}}^T \underline{D}_{mb,ep}^{co} \hat{\underline{N}} \right]^{-1} \hat{\underline{N}}^T \underline{D}_{mb,ep}^{co} \right\} \quad (33)$$

where $\underline{D}_{mb,ep}^{co}$ was defined in (21).

2.3 - Reinforcement material constitutive laws

In the present model a plain or fibrous concrete laminate structure can be reinforced with sets of smeared steel bars. The stress-strain relationship of a steel bar can be simulated by a linear-parabola diagram or by a multilinear diagram⁹. The material non-linear behaviour of a steel bar is reproduced under the elasto-plasticity framework⁹.

2.4 - Tension stiffening model

A tension-stiffening model was developed for laminar concrete structures that can be reinforced with several sets of smeared bars with different orientation and properties. This model is based on the principles proposed by Link *et al.*²⁵ and Massicotte *et al.*²⁶, and can be represented by the post-peak stress-strain trilinear diagram illustrated in Figure 3. The

definition of the characteristic points A, B and C of the tension-stiffening diagram is discussed on a previous work⁹.

Tensile behaviour of cracked concrete layer is governed by a stiffening or a softening law, if this layer is under the influence of a reinforcement set or it is not under the influence of any reinforcement set, respectively. To verify if a cracked concrete layer is in softening or is in a stiffening state, a criteria was established. According to this criteria, a cracked concrete layer is in stiffening if its middle surface is in the effective thickness, h_{ef} (see Figure 4), evaluated from the recommendations of the CEB-FIP Model Code 1990¹⁹. The cracked concrete layers outside the effective thickness are in softening state.

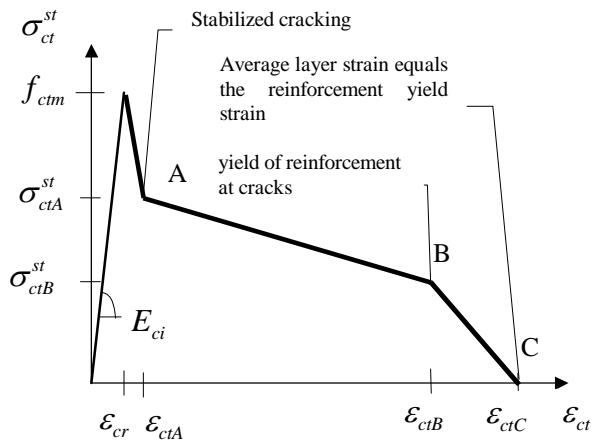


Figure 3 : Tension-stiffening diagram⁹.

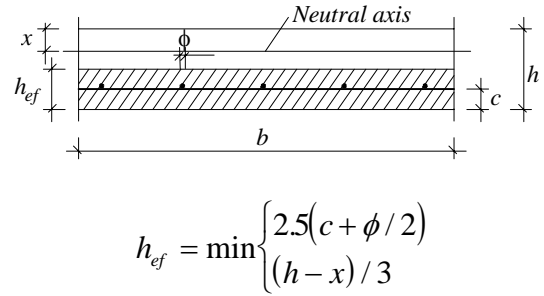


Figure 4 : Evaluation of the effective thickness according to CEB-FIP Model Code 1990¹⁹.

2.5 Soil

The soil is simulated by springs orthogonal to the laminate structure (see Figure 5). The tangent soil reaction modulus is usually evaluated from plate-loading tests²⁷. The results of these tests reveal that soil pressure–settlement relationship may be simulated with a multilinear or linear-parabola diagram⁹. The soil contribution to the stiffness of the whole structural system is computed adding the soil stiffness matrix,

$$\underline{K}_{so}^{(e)} = \int_{A^{(e)}} \underline{R}^T k_s \underline{R} dA \quad (34)$$

to the reinforced concrete stiffness, where $A^{(e)}$ is the area of the finite element, \underline{R} is a vector with a dimension of the element nodes and including the values of the shape functions, and k_s is the tangent soil reaction modulus⁹. If in a given sampling point the concrete slab loses

the contact with the soil (see Figure 6), i.e., if the descendent vertical displacement of the slab middle surface, \bar{u}_3 , is less than the plastic soil settlement, a_{sp} , the part of the soil corresponding to this sampling point does not contribute to the stiffness of the slab-soil system.

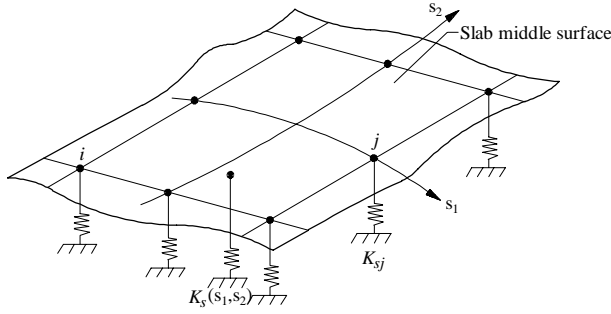


Figure 5 : The soil is discretized by spring elements orthogonal to the concrete slab middle surface.

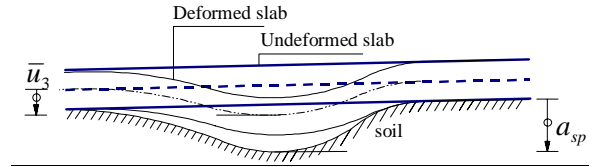


Figure 6 : Loss of contact between the slab and the soil is accounted for.

3. APPLICATIONS

3.1 Introduction

The ability of the present model to simulate the behaviour of concrete slabs supported on soil was already demonstrated in other publications^{5,9,28}. The main objective of the present section is to confront linear and non-linear approaches to design an industrial floor. In a first step, the slab floor will be designed using a linear finite element computational code²⁹. This is the common approach used in the practice. In a second step, the load bearing capacity of this pavement is evaluated by applying the model described in chapter 2. In a third step it is determined the amount of steel fibres that is equivalent to the conventional reinforcement obtained. The behaviour of the slab reinforced with steel fibres is compared with the behaviour of the slab reinforced with conventional reinforcement. The influence of the soil bearing capacity on the slab-soil structural behaviour is analysed for the wire mesh reinforced concrete slab and for the *SFRC* slab. The safety factors are discussed. The last study focuses the influence of the loss of contact between the slab and the soil.

3.2 Designing the reinforcement by a linear elastic finite element code

To design the slab represented in Figure 7, a quarter of it was discretized by eight-noded isoparametric plane shell elements. The mesh is shown in Figure 8. This slab has 120 mm thickness and is loaded in four areas of 350x350 mm², representing the loading of a truck. The design load of each wheel of a truck is 57.5 kN, and is distributed on the area of a finite

element, as is it schematically represented in Figure 8. The design values of the material properties are included in Table 2. Using a model to design smeared reinforcement for shell concrete structures²⁹, it was obtained a reinforcement of $142 \text{ mm}^2/\text{m}$ in x_1 and x_2 direction, placed at 20 mm from slab bottom surface.

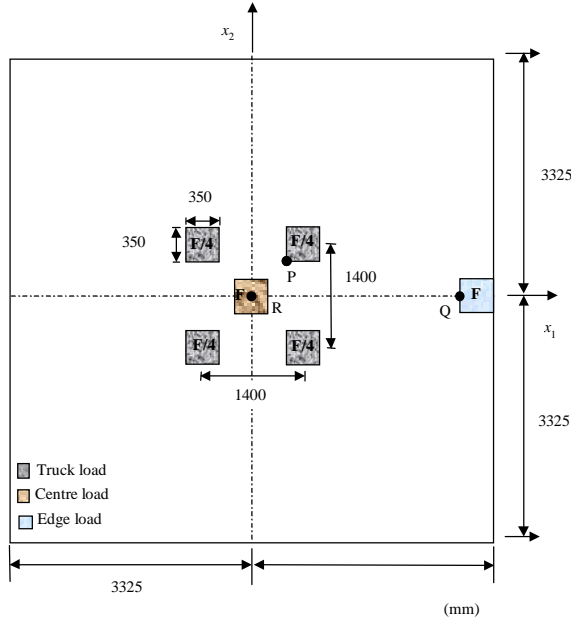


Figure 7 : Slab geometry and loading.

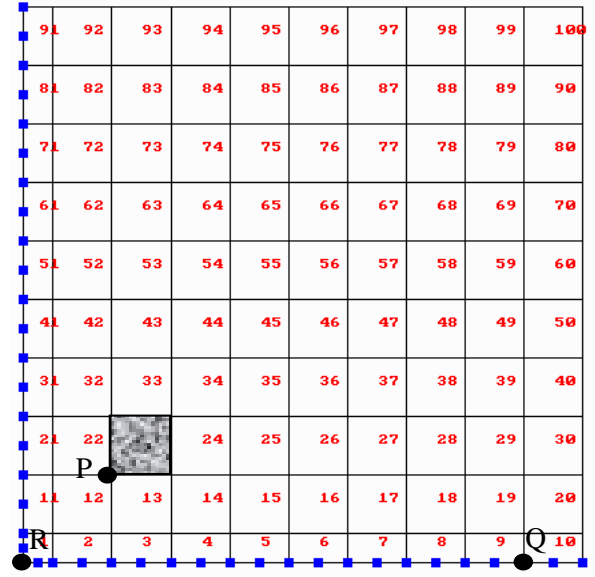


Figure 8 : Finite element mesh.

Concrete	Reinforcement	Soil
$E_c = 26\,000 \text{ MPa}$, $\nu = 0.15$ $f_{cd} = 11.333 \text{ MPa}$ $G_f = 0.06 \text{ N.mm}$, $l_b = 45 \text{ mm}$	$f_{syd} = 435 \text{ MPa}$, $E_s = 200\,000 \text{ MPa}$	$k_s = 0.06 \text{ N/mm}^3$

Table 2 : Values of the material properties.

3.2 Steel fibre content equivalent to a given conventional reinforcement

A multilayer model was used to evaluate the fibre content equivalent to conventional reinforcement obtained in last section ($142 \text{ mm}^2/\text{m}$). The thickness of the cross sectional area of a unit length of the slab was subdivided in ten layers. The behaviour of each concrete layer and the behaviour of the reinforcement were simulated with the constitutive laws described in chapter 2 of the present work. A full description of the cross section multilayer model can be found elsewhere¹⁴. Using the data included in Table 2 it was verified that 40 Kg/m^3 of

ZX60/.80 hooked ends steel fibres provides a maximum resisting moment similar to the maximum resisting moment registered in the cross section reinforced with the wire mesh. It should be pointed that the *SFRC* slabs have identical resistance under positive and negative moments, which is equivalent to slabs conventionally reinforced in both faces ($2 \times 142 = 284 \text{ mm}^2/\text{m}$).

3.3 Material non-linear analysis

In this section the slab reinforced with a wire mesh of $142 \text{ mm}^2/\text{m}$, placed at 20 mm from slab bottom surface, is analysed using the model described in chapter 2. In this analysis the material properties were defined from their characteristic values, included in Table 3. Two soils with different ultimate resisting pressures were used in order to evaluate the influence of the soil constitutive law on the slab-soil response. It was admitted that the soil pressure at the beginning of soil non-linearity is the maximum soil pressure registered in the linear finite element analysis (0.036 MPa). Parameter β (see Figure in Table 3) defines the beginning of the soil non-linearity.

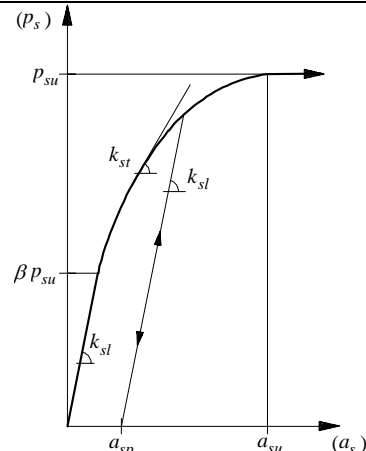
Concrete	Soil
$E_c = 30\,000 \text{ MPa}$ $\nu = 0.15$ $f_{ck} = 20 \text{ MPa}$ $f_{ctk} = 1.6 \text{ MPa}$ $l_b = \text{square root of the Gauss point area}^{10}$ Plain concrete: $G_f = 0.06 \text{ N.mm}$ $\alpha = 0.3; \xi = 0.1$ (bilinear softening diagram) <i>SFRC</i> : $G_f = 2.068 \text{ N.mm}$ $\alpha_1 = 0.55; \xi_1 = 0.004; \alpha_2 = 0.25; \xi_2 = 0.2$	 <p style="text-align: center;"> $k_s = 0.06 \text{ N/mm}^3, \beta p_{su} = 0.036 \text{ MPa}$ soil 1: $p_{su} = 0.4 \text{ MPa}, \beta = 0.09, a_{su} = 13.33 \text{ mm}$ soil 2: $p_{su} = 0.1 \text{ MPa}, \beta = 0.36, a_{su} = 3.33 \text{ mm}$ </p>
Reinforcement	
$f_{syd} = 500 \text{ MPa}$ $E_s = 200\,000 \text{ MPa}$	

Table 3 : Characteristic values of the material properties

The relationship between the total load and the descending vertical displacement of point P (see Figure 7) for slabs reinforced with wire mesh and for *SFRC* slabs is depicted in Figure 9.

It can be verified that *SFRC* slabs has a load bearing capacity greater than wire mesh reinforced concrete slabs, for both soils, in spite of the cross section multilayer model has predicted similar flexural strength.

From Figure 9 it can be observed that by enhancing the soil load bearing capacity, an increase on the failure load of the *SFRC* slab over wire mesh reinforced concrete slab is obtained. This tendency should be related to the higher energy absorption capacity and better stress redistribution of *SFRC*. It should be pointed out that the load configuration under consideration is not the most unfavourable for design purposes.

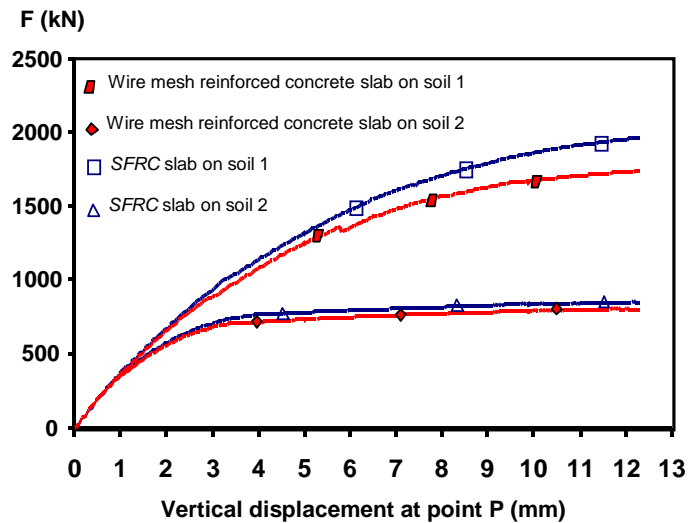


Figure 9 : Total force-displacement relationship.

The relationship between the load and the displacement at point Q (see Figure 7) for the load placed at the centre of the slab (distributed in a area of $350 \times 350 \text{ mm}^2$) and the relationship between the load and the displacement at point R (see Figure 9) for the load placed at the middle of the slab edge are depicted in Figures 10 and 11, for the slabs reinforced with wire mesh. It is shown that the load placed at the middle of the slab edge is the most unfavourable load configuration. The load at a slab corner should be also analysed.

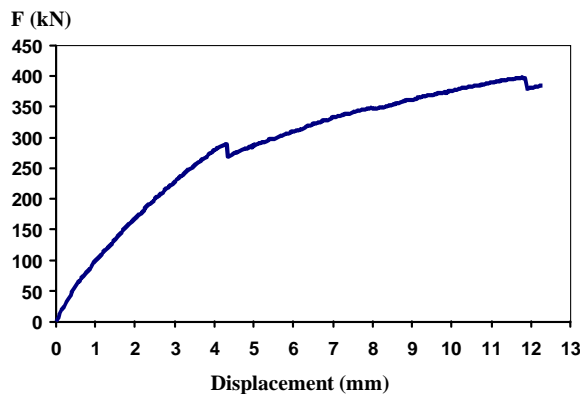


Figure 10 – Load-displacement at point R (see Figure 9) for load in the centre of the slab.

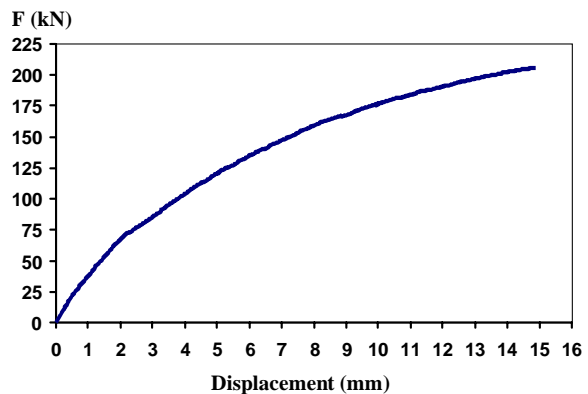


Figure 11 – Load-displacement at point Q (see Figure 9) for load in the middle of the slab edge.

Figures 12 and 13 depict the crack patterns on top and bottom concrete layers for wire mesh reinforced concrete slab supported on soil 1 and soil 2, respectively. The width of the

rectangle representing the smeared cracks at a sampling point is proportional to the normal crack strain, and consequently, it is proportional to the crack opening. The completely open crack is represented by blue colour, while the cracks in the other states (softening, closing, reopening and completely closed) are represented by red colour. In these figures it is also depicted probable “failure lines” by thick lines. For the slab supported on soil 1, a more diffuse cracking pattern is observed leading to the development of several “failure lines”. In slab supported on soil 2 the cracking damage is concentrated near the element loaded. Less number of “failure lines” arises in this case.

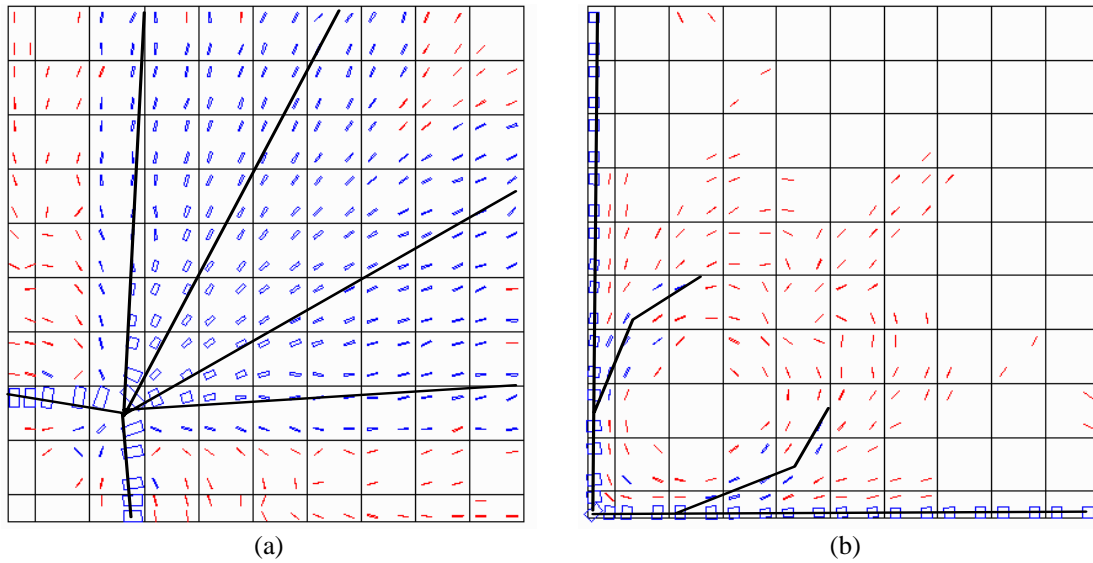


Figure 12 : Crack patterns on bottom (a) and top (b) concrete layer of wire mesh reinforced concrete slab supported on soil 1.

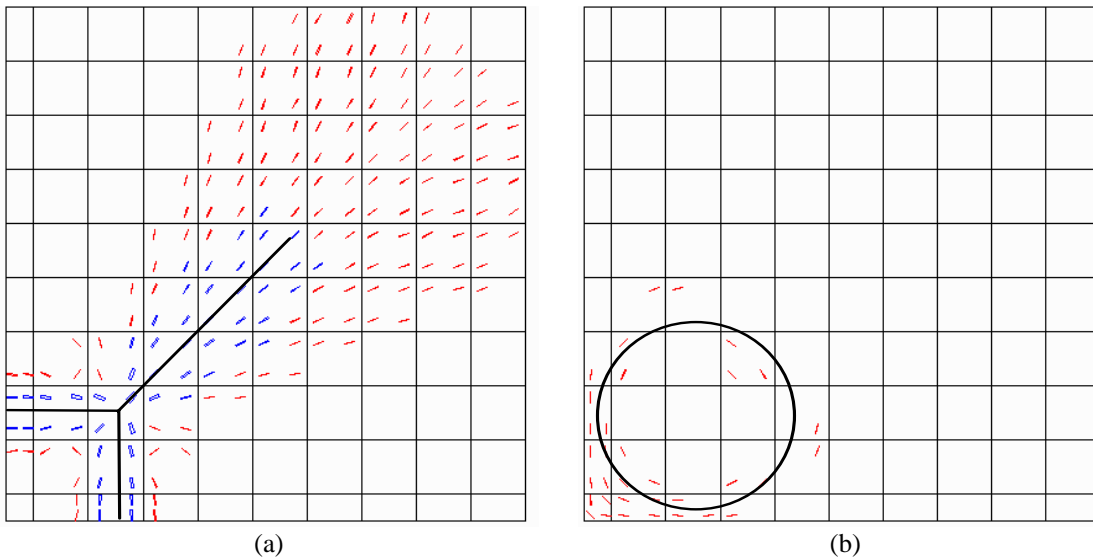


Figure 13 : Crack patterns on bottom (a) and top (b) concrete layer of wire mesh reinforced concrete slab supported on soil 2.

Figures 14 and 15 represent the crack patterns on top and bottom concrete layers of *SFRC* concrete slab supported on soil 1 and 2, respectively. Due to the higher fracture energy, all the cracks are completely opened (the fracture energy is exhausted). This fact is responsible for the higher load bearing capacity of *SFRC* slabs, in comparison to the load bearing capacity of the wire mesh reinforced concrete slabs. The configuration of the “fracture lines” on *SFRC* slabs are similar to that represented in the wire mesh reinforced concrete slabs.

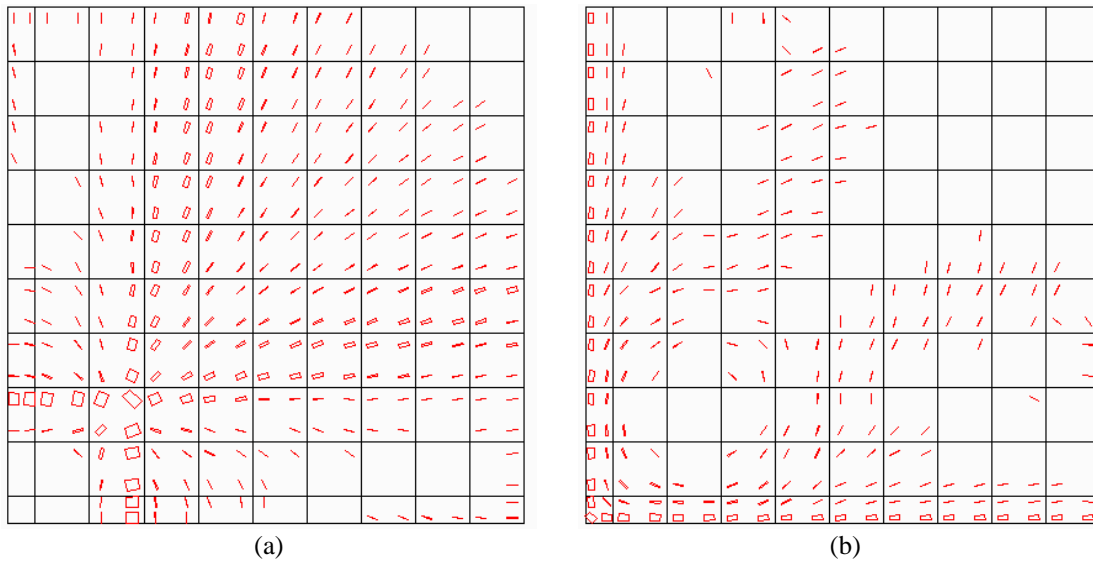


Figure 14 – Crack patterns on bottom (a) and top (b) concrete layer of *SFRC* concrete slab supported on soil 1.

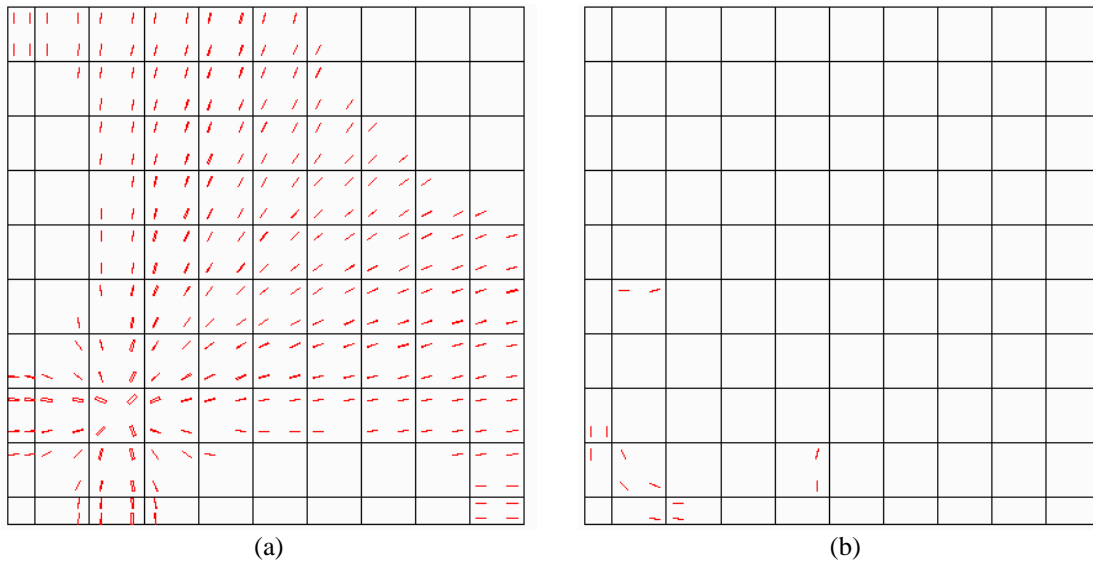


Figure 15 – Crack patterns on bottom (a) and top (b) concrete layer of *SFRC* concrete slab supported on soil 2.

For truck load configuration, the ultimate load of the slabs analysed is included in Table 4, as well as the safety factor (the design load is $4 \times 57.5 = 230$ kN). Safety factors increase significantly with the soil load bearing capacity. Designing a slab supported on a soil of usual bearing capacity, using a linear elastic finite element computer code leads to very high safety factor.

	Wire mesh reinforced concrete slab		<i>SFRC</i> slab	
	Soil 1	Soil 2	Soil 1	Soil 2
Maximum load (kN)	1730	800	1950	850
Safety factor	7.5	3.5	8.5	3.7

Table 4 – Ultimate loads and safety factor values.

3.4 Influence of the loss of contact between the slab and the soil

The slabs were once more analysed with the material non-linear finite element model, but now without simulating the loss of contact between the slab and the soil, i.e., it is admitted that the soil behaves in tension like in compression. The force-displacement relationship is depicted in Figure 16. It can be concluded that the simulation of the loss of contact between the slab and the soil must be taken into account, otherwise an unsafe failure load will be estimated. This effect is increased with the soil load bearing capacity.

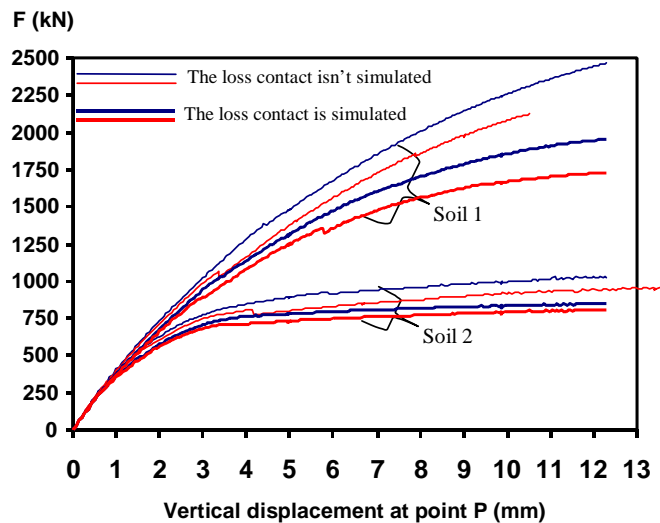


Figure 16 : The influence of the loss of contact between the slab and the soil.

4 CONCLUSIONS

A model was described for material non-linear analysis of concrete slabs supported on soil. This model has shown that designing with linear elastic finite element codes leads to very high safety factors, even in soils with standard load bearing capacities. The slab-soil system is very sensitive to the soil constitutive law. The failure load increases significantly with the soil bearing capacity.

Using a cross sectional multilayer model, a content of fibres was obtained in order to give a flexural strength similar to that of a section reinforced with a given conventional reinforcement percentage. The high load bearing capacity and the better cracking behaviour registered on steel fibre reinforced concrete slabs, when compared to wire mesh reinforced concrete slabs, shows that the equivalent fibre content should be obtained in an energetic basis, not in a flexural basis.

The results, which were presented, reveal that it is important to simulate the loss of contact between the slab and the soil, otherwise failure loads will be artificially increased.

REFERENCES

- [1] A. Nanni and A. Johari, "RCC pavement reinforced with steel fibers", *Concrete International*, 64-69, April, (1989).
- [2] C. Robinson, A. Colasanti and G. Boyd, "Steel fibers reinforced auto assembly plant floor", *Concrete International*, 30-35, April, (1991).

- [3] P.C. Tatnall and L. Kuitenbrouwer, "Steel fiber reinforced concrete in industrial floors", *Concrete International*, 43-47, December, (1992).
- [4] H. Falkner and M. Teutsch, *Comperative investigations of plain and steel fibre reinforced industrial ground slabs*, Institut Fur Baustoffe, Massivbau und Brandschutz, N° 102, (1993).
- [5] J.A.O. Barros and J.A. Figueiras, "Experimental behaviour of fiber concrete slabs on soil", *Journal Mechanics of Cohesive-frictional Materials*, **3**, 277-290, (1998).
- [6] H.M. Westergaard, "Stresses in concrete pavements computed by theoretical analysis", *Publ. Roads* **7**, (1926-27).
- [7] A. Losberg, *Design methods for structurally reinforced concrete pavements*, Transactions of Chalmers University of Technology Gothenburg, Sweden, (1961).
- [8] G.G. Meyerhof, "Load carrying capacity of concrete pavements", *Journal of the Soil Mechanics and Foundations Division*, June, (1962).
- [9] J.A.O.Barros, *Comportamento do betão reforçado com fibras - análise experimental e simulação numérica* PhD dissertation, Civil Eng. Dept., Faculty of Engineering, University of Oporto, Portugal (in Portuguese), (1995).
- [10] Rots, J.G., *Computational modeling of concrete fracture*, PhD Dissertation, Delft University of Technology, (1988).
- [11] R. De Borst and P. Nauta, "Non-orthogonal cracks in a smeared finite element model", *Eng. Computations*, **2**, 35-46, March, (1985).
- [12] E. Reissner, "The effect of transverse shear deformation on the bending elastic plates", *Jour. Appl. Mech.*, **12**, 69-76, (1945).
- [13] T.S. Chow, "On the propagation of flexural waves in an orthotropic laminated plate and its response to an impulsive load", *Jour. of Composite Materials*, **5**, 306-319, (1971).
- [14] J.A.O. Barros, J.A. Figueiras, "Flexural behavior of steel fiber reinforced concrete: testing and modelling", *Journal of Materials in Civil Engineering*, ASCE. (accepted to be published)
- [15] Bekaert Specification, *Dramix fibres hors fils d'acier pour reinforcement de betón et mortier*, Bekaert N.V., (1991).
- [16] RILEM TC 50-FMC, "Determination of fracture energy of mortar and concrete by means of three-point bend tests on notched beams", *Materials and Structures*, **18(106)**, 285-290, (1985).
- [17] V.S. Gopalaratnam and S.P. Shah, "Tensile failure of steel fibre-reinforced mortar", *Jour. of Eng. Mech.*, ASCE, **113(5)**, 635-653, May, (1987).
- [18] V. Cervenka, H. Pukl and R. Eligehausen, "Computer simulation of anchoring technique and design of concrete structures", *Proc. Second Intern. Conf. on Computer Aided Analysis and Desing of Concrete Structures, Zell am See, Austria*, 1-19, (1990).

- [19] CEB-FIP Model Code 1990. *Comite Euro-International du Beton*, Bulletin d'Information n° 213/214, Ed. Thomas Telford, (1993).
- [20] G. Hofstetter and H.A. Mang, *Computational mechanics of reinforced concrete structures*, Ed. Vieweg, (1995).
- [21] W. S. Yin, E.C.M. Su, M.A. Mansur and T.T.C. Hsu, "Biaxial tests of plain and fiber concrete", *ACI Materials Journal*, **86(3)**, 236-243, May-June (1989).
- [22] L.A. Traina, S.A. Mansour, "Biaxial strength and deformational behaviour of plain and steel fiber concrete", *ACI Materials Journal*, **88(4)**, 354-363, July-Aug. (1991).
- [23] Figueiras, J.A., *Ultimate load analysis of anisotropic and reinforced concrete plates and shells*, Ph.D. Thesis, C/Ph/72/83, Uni. College of Swansea, (1983).
- [24] Feenstra, P.H., *Computational aspects of biaxial stress in plain and reinforced concrete*, PhD Thesis Delft University of Technology, (1993).
- [25] R.A. Link, A.E. Elwi, A. Scanlon, "Biaxial tension stiffening due to generally oriented reinforced layers", *Jour. of Eng. Mech., ASCE*, **115(8)**, 1647-1662, August, (1989).
- [26] B. Massicote, A.E. Elwi, J.G. MacGregor, "Tension-stiffening model for planar reinforced concrete members", *Jour. of Struct. Eng., ASCE*, **116(11)**, 3039-3058, November, (1990).
- [27] ASTM D 1194-72, *Bearing capacity of soil for static load and spread footing*, (1972).
- [28] J.A. Barros and J.A. Figueiras, "Simulação numérica do comportamento de lajes de betão reforçado com fibras de aço apoiadas em solo", *6º Encontro Nacional sobre Estruturas Pré-Esforçadas*, Lisboa, LNEC, 1-57 a 1-70, Novembro, (1996).
- [29] Alvaro F.M. Azevedo and J.A. Barros, *Manual de utilização do programa FEMIX-versão 3.0*, FEMopen Consultoria e Software de Engenharia, 1998.